

Compact User-Side Reconfigurable Intelligent Surfaces for Uplink Transmission

Kunzan Liu, Zijian Zhang, Linglong Dai, and Lajos Hanzo

Abstract

Large-scale antenna arrays employed by the base station (BS) constitute an essential next-generation communications technique. However, due to the constraints of size, cost, and power consumption, it is usually considered unrealistic to use a large-scale antenna array at the user side. Inspired by the emerging technique of reconfigurable intelligent surfaces (RIS), we firstly propose the concept of user-side RIS (US-RIS) for facilitating the employment of a large-scale antenna array at the user side in a cost- and energy-efficient way. In contrast to the existing employments of RIS, which belong to the family of base-station-side RISs (BSS-RISs), the US-RIS concept by definition facilitates the employment of RIS at the user side for the first time. This is achieved by conceiving a multi-layer structure to realize a compact form-factor. Furthermore, our theoretical results demonstrate that, in contrast to the existing single-layer structure, where only the phase of the signal reflected from RIS can be adjusted, the amplitude of the signal penetrating multi-layer US-RIS can also be partially controlled, which brings about a new degree of freedom (DoF) for beamformer design that can be beneficially exploited for performance enhancement. In addition, based on the proposed multi-layer US-RIS, we formulate the signal-to-noise ratio (SNR) maximization problem of US-RIS-aided communications. Due to the non-convexity of the problem introduced by this multi-layer structure, we propose a multi-layer transmit beamformer design relying on an iterative algorithm for finding the optimal solution by alternately updating each variable. Finally, our simulation results verify the superiority of the proposed multi-layer US-RIS as a compact realization of a large-scale antenna array at the user side for uplink transmission.

K. Liu, Z. Zhang, and L. Dai are with the Beijing National Research Center for Information Science and Technology (BNRist) as well as the Department of Electronic Engineering, Tsinghua University, Beijing 100084, China (e-mails: lkz18@mails.tsinghua.edu.cn, zhangzj20@mails.tsinghua.edu.cn, daill@tsinghua.edu.cn).

L. Hanzo is with the Department of Electronics and Computer Science, University of Southampton, Southampton SO17 1BJ, U.K. (e-mail: lh@ecs.soton.ac.uk).

Index Terms

Reconfigurable intelligent surfaces (RIS), user-centric, large-scale antenna arrays, multi-layer structure, transmit beamformer design.

I. INTRODUCTION

The internet of things (IoT) has attracted much research interest in the communication community. In next-generation networks, the number of access points may reach millions per square kilometer in tele-traffic hotspots [1]. The interactions among smart devices, such as robots, intelligent reconfigurable furniture, and vehicles will require increasing wireless communications quality. In downlink transmissions, massive multiple-input multiple-output (MIMO) systems boost the capacity by employing a large-scale array having hundreds of antennas at the base station (BS) side [2]. It has been verified that massive MIMO systems are capable of achieving orders of magnitude increase in spectral efficiency by simultaneously serving a massive number of users [3].

However, in uplink transmissions, employing a large-scale array at the user side has been considered as unrealistic. Although a large-scale beamformer generates high-gain beams, which increases the channel capacity and enhances the wireless coverage, there is a fundamental dimensionality limit that prevents this idea. Specifically, traditional antenna arrays require numerous radio-frequency (RF) components, like RF chains in the fully digital architecture [4] and phased arrays in the hybrid architecture [5]. Hence this would lead to bulky circuits, high hardware cost, and excessive power consumption at the user side.

As a remedy, the emerging innovative technique of reconfigurable intelligent surfaces (RIS) constituted by a large-scale array developed from meta-materials may be harnessed [6], [7]. The appeal of RISs is that they can enhance the communications in a cost- and energy-efficient way, which provides us with a promising opportunity to construct large-scale arrays in a compact form at the user side.

A. Prior contributions

Again, a RIS is a large-scale array composed of a large number of low-cost elements, which can reflect or transmit the incident electromagnetic waves in the desired directions by appropriately adjusting their phase shifts [8], [9]. In contrast to the traditional energy-hungry RF components, the RISs are nearly passive, which can engender the required phase shifts in an energy-efficient

way [10], [11]. Since the benefits of RISs have already been verified in practical wireless communications prototypes [12], [13], RISs have been regarded as a promising technique for future 6G wireless communications [14].

The applications of RISs can be generally divided into two broad categories. The first category employs relay-like RISs between the BS and the user for enhancing the transmission links. For example, RISs can provide additional propagation paths and thus can be utilized for improving the transmission reliability by overcoming blockages [8]. Another scenario is considered where multiple BSs and multiple RISs are employed for simultaneously serving multiple users. As a benefit, compared to traditional networks operating without RISs, an improved network capacity and energy efficiency can be achieved [15]–[17]. In [18], RISs are used for reducing the transmit power of the BS, which is derived by jointly optimizing the phase shifts of RIS elements as well as the parameters of both the BSs and users.

The second category employs RISs near the BS for analog beamforming at a low cost and frugal power consumption. The authors of [19] propose a RIS-based transmit precoding architecture for maximizing the sum-rate, where the phased arrays are replaced by the RIS at the BS side. As a further development, the authors of [20] utilize a RIS at the BS side for beamforming relying on the optimal phase shifts. In these contributions, RISs serve as part of a new BS type that transmits/receives signals at a reduced cost and power consumption [19], [20].

In a nutshell, both the above two categories utilize RISs for improving the communication performance of the cellular network, hence we refer to them as base-station-side RISs (BSS-RISs). By contrast, RISs have not been employed at the user side in the open literature.

B. Our contributions

To circumvent the dimensionality limit of employing a large-scale array at the user side, we propose the concept of user-side RISs (US-RISs), where the RIS is employed at the user side for enhancing the user's capability in uplink transmissions. Specifically, the contributions of this paper can be summarized as follows.

- We propose the concept of US-RIS to break the dimensionality limit and to facilitate the employment of a large-scale array at the user side. In contrast to the existing BSS-RISs, which are utilized for improving the communication performance of the cellular network, this is the first use case of RIS dedicated to the user side.

- We propose and analyze a multi-layer structure to realize US-RISs by considering the space-limited characteristics of users. Explicitly, in contrast to existing RISs, where only the phase of the signal can be adjusted, the amplitude of the signal can also be partially controlled. This provides us with an additional degree of freedom (DoF) for RIS beamforming design.
- We then formulate the associated signal-to-noise ratio (SNR) maximization problem of US-RIS-aided communications. Due to the non-convexity introduced by the multi-layer RIS structure proposed, we develop a multi-layer transmit beamformer design that can control both the phase and the amplitude of the transmitted signal. Specifically, the proposed multi-layer transmit beamformer design relies on an iterative optimization algorithm for finding the optimal solution to the problem formulated. Finally, our simulation results verify the benefits of the proposed multi-layer US-RIS as a realization of a large-scale array at the user side for uplink transmission.

C. Organization and notation

Organization: The rest of the paper is organized as follows. In Section II, we propose the basic concept of US-RIS. Then, we conceive a novel architecture relying on this multi-layer US-RIS. In Section III, we theoretically analyze the performance of the proposed multi-layer structure. In Section IV, we consider a US-RIS-aided communications scheme and formulate the corresponding SNR maximization problem. The multi-layer transmit beamformer design is proposed as an iterative algorithm for solving the problem formulated, where each variable is updated in an alternating fashion. In Section V, simulation results are provided for quantifying the performance of US-RIS-aided communications, demonstrating the practical realization of a large-scale array at the user side for uplink transmission. Finally, in Section VI, we provide our conclusions followed by promising future research ideas.

Notation: \mathbb{C} , \mathbb{R} , and \mathbb{R}_+ denote the set of complex, real, and positive real numbers, respectively; $[L]$ represents the set of integers $\{1, 2, \dots, L\}$; \mathbf{A}^{-1} , \mathbf{A}^* , \mathbf{A}^T , and \mathbf{A}^H denote the inverse, conjugate, transpose, and conjugate transpose of matrix \mathbf{A} , respectively; $\|\mathbf{x}\|_2$ is the ℓ_2 -norm of vector \mathbf{x} ; $\langle \mathbf{x} \rangle$ is the normalized vector of \mathbf{x} , i.e., $\langle \mathbf{x} \rangle = \mathbf{x}/\|\mathbf{x}\|_2$; $\arg(\mathbf{x})$ and $\exp(\mathbf{x})$ denote the phase angle and exponential representation of each element of the complex vector \mathbf{x} , respectively; $|x|$ denotes the amplitude of a complex scalar x ; $\text{diag}(\cdot)$ is the diagonal operation; $\mathcal{CN}(\boldsymbol{\mu}, \boldsymbol{\Sigma})$ represents the complex multivariate Gaussian distribution with the mean $\boldsymbol{\mu}$ and the variance

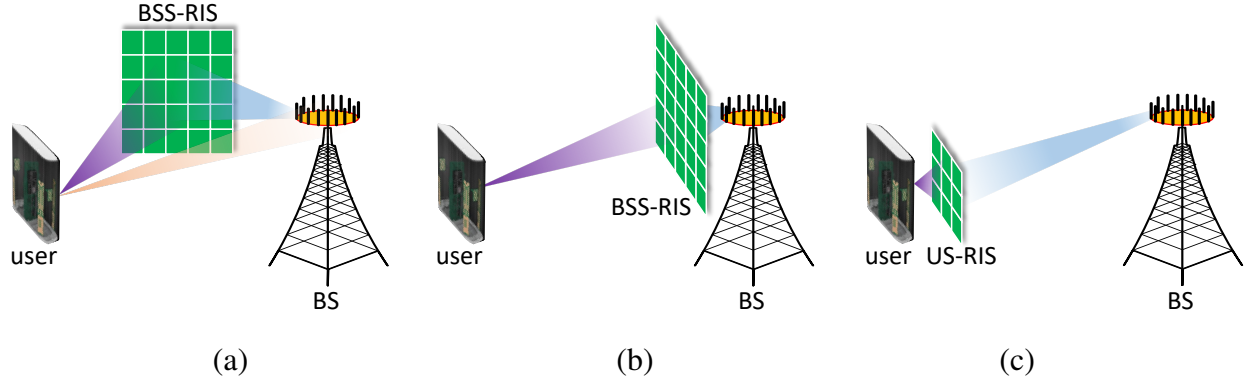


Fig. 1. Different communication systems utilizing RIS. (a) BSS-RIS-aided communications, where a relay-like RIS is employed between the BS and the user for enhancing the multipath diversity by mitigating blockages. (b) BSS-RIS-aided communications, where the RIS is employed at the BS side. (c) US-RIS-aided communications, where the RIS is employed at the user side.

Σ ; $\mathbf{0}_L$ denotes the $L \times 1$ zero vector; \mathbf{I}_L denotes the $L \times L$ identity matrix; $\psi_{\max}(\mathbf{A})$ is the eigenvector of matrix \mathbf{A} corresponding to its largest eigenvalue.

II. SYSTEM MODEL

To realize a large-scale array at the user side at a low cost and low power consumption, in this section, we propose the concept of US-RISs. Specifically, the concept is introduced in Subsection II-A. Then, we propose a novel architecture relying on a multi-layer US-RIS and compare it to existing BSS-RISs in Subsection II-B. Finally, in Subsection II-C, we develop the system model of US-RIS-aided communications.

A. Concept of US-RIS

As the terminology suggests, US-RIS is a hardware technique conceived for constructing a large-scale array at the user side.

Again, traditional applications of RISs in wireless communications are limited to employing RISs between the BS and the user or alternatively, at the BS side, as shown in Fig. 1 (a) and (b), respectively. In Fig. 1 (a), a relay-like RIS is used to “reconfigure” the wireless channels for enhancing the multipath diversity by mitigating blockages. By contrast, in Fig. 1 (b), a RIS is employed at the BS side for beamforming. Again, both of these two applications aim for improving the performance of the cellular network, which are termed as BSS-RISs.

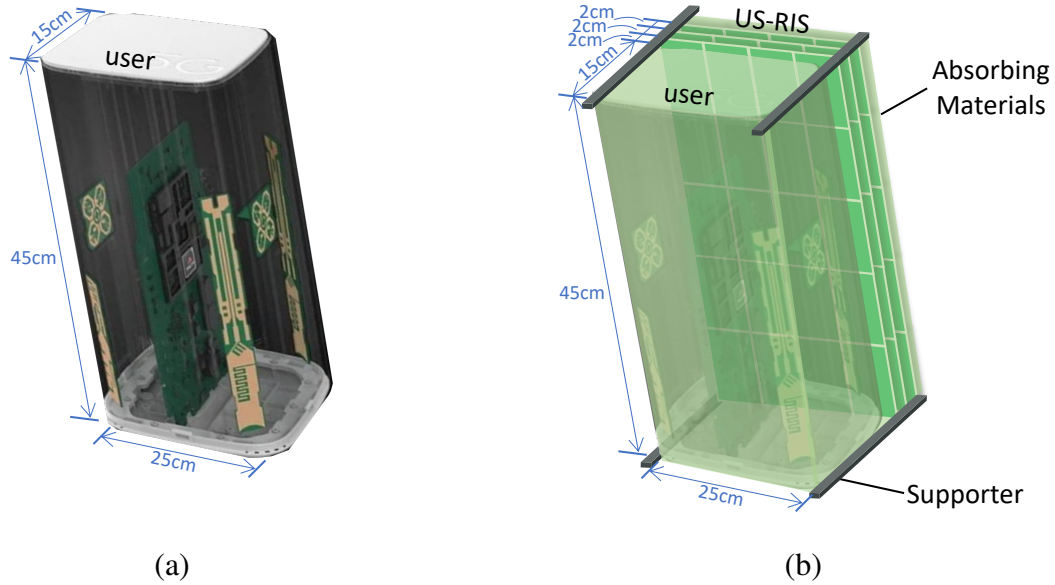


Fig. 2. US-RIS construction. (a) A typical user which is a real-world model of customer-premises equipment (CPE). (b) The proposed architecture with multi-layer US-RIS.

By contrast, here we conceive the US-RIS concept shown in Fig. 1 (c). In contrast to the traditional BSS-RISs, US-RISs are employed close to the user as a realization of a large-scale array at the user side. Given their cost- and energy-efficient characteristics, US-RISs are eminently suitable for compact user-side employment, which dispels the myth that a user can hardly harness a large-scale array, considering the inherent cost- and power-constraints.

B. Architecture

To illustrate a potential US-RIS construction, Fig. 2 gives an example based on a customer-premises equipment (CPE). Specifically, this CPE facilitates access to communication routers, network switches, and networking adapters. Fig. 2 (a) portrays a real-world CPE model of size $25\text{ cm} \times 15\text{ cm} \times 45\text{ cm}$. The physical size of this transmissive US-RIS is beneficially reduced by constructing a multi-layer structure. Fig. 2 (b) shows the axonometric construction of the US-RIS, where three layers of RISs are vertically stacked in front of the CPE in order to form a multi-layer structure, with a 2 cm gap between adjacent vertical layers. In this way, the overall size of the resultant US-RIS-aided CPE becomes $25\text{ cm} \times 21\text{ cm} \times 45\text{ cm}$, which may be deemed acceptable for a domestic installation. Note that the number of layers and the inter-layer gaps are flexible for practical applications. Naturally, the entire structure should be hosted by an enclosure, surrounded by absorbing materials to reduce the energy loss and to protect the internal channel

TABLE I
COMPARISON BETWEEN BSS-RIS AND US-RIS

| Aspect | BSS-RIS | US-RIS |
|----------------|----------------------|--------------------|
| Location | BS | user |
| Controller | one/multiple BS(s) | one user |
| Beneficiary | one/multiple user(s) | one user |
| Operating mode | mainly reflective | transmissive |
| Structure | single-layer | single/multi-layer |
| Size | large | compact |
| EAR | small | big |

from external interference. As usual, the controller is informed by the channel estimator on how to configure the phase shifts of US-RISs.

To clarify the characteristics of this novel user-side architecture and the differences between BSS-RIS and US-RIS, we summarize their key aspects in Tab. I and compare them as follows.

- *Location, controller, and beneficiary:* According to their terminologies, the most essential difference between BSS-RIS and US-RIS is their location. The BSS-RIS is primarily proposed for improving the overall channel capacity of the cellular network, while US-RIS at the user side is transmissive and may also be regarded as an integral component of the user. Hence, both the controller and the beneficiary of the BSS-RIS and US-RIS are different. The BSS-RIS is controlled by one/multiple BS(s) in the system and it cooperatively serves one/multiple user(s) at the same time. By contrast, for the US-RIS, both the controller and the beneficiary is the same user. Both the beamforming design and phase-shift control are carried out at the US-RIS.
- *Operating mode and structure:* Most BSS-RISs tend to be reflective arrays [15], [16], [18], [19], while our US-RIS is a transmissive array operating under a tight space constraint at the user side [21]. The multi-layer structure is conceived for further improving the array gains attained in a limited space. To elaborate, in contrast to the existing single-layer structure, which can only adjust the phase of the incident signal, our multi-layer structure has the advantage that it facilitates partial amplitude control of the radiated signals. This feature

provides a new DoF for beamforming design, which will be detailed in Section III.

- *Size and element activation ratio (EAR):* In BSS-RIS-aided communications, the size of the BSS-RIS is expected to be large, which is not practical for the user-side. To limit the user's total size, each layer of the US-RIS should be much smaller than a BSS-RIS. However, the proposed multi-layer structure is capable of alleviating the disadvantages of compact size. Concretely, the multi-layer RIS simultaneously controls the phase shifts of the different RIS layers. We now proceed by introducing the new metric of element activation ratio (EAR), which explicitly quantifies the particular fraction of activated elements of a transmissive RIS. Specifically, in this ratio, we count an element as being “activated”, if its power is higher than a threshold percentage ε of the average power¹. In Subsection V-D, we will provide experimental EAR results. Apart from the compact structure of our US-RIS, a further particular benefit of the proposed multi-layer structure is that it is capable of reducing the pilot overhead required for channel estimation, since the channels experienced by the parallel US-RIS layers are similar and can be estimated in advance.

C. System model of US-RIS-aided communications

Let us consider the US-RIS-aided communications scenario of Fig. 3, where a multi-layer US-RIS is used for enhancing the uplink transmission from the user to the BS. Assume furthermore that the user and the BS are equipped with K transmit antennas (TAs) and M receive antennas (RAs), respectively. The US-RIS is composed of L layers having N_l elements on the l -th layer. Without loss of generality, we assume² that N_l is equal to N for all $l \in [L]$. Finally, we denote the n -th TA element on the US-RIS's l -th layer as the (l, n) -th TA element.

We denote the transmitted uplink symbol by $s \sim \mathcal{CN}(0, 1)$. The symbol s is firstly processed by the uplink transmit beamforming (UL-TBF) vector $\mathbf{w} \in \mathbb{C}^{K \times 1}$ of Fig. 3, subject to the power constraint $\|\mathbf{w}\|_2^2 \leq P_{\max}$ before transmission. Only the UE-RIS-BS line-of-sight (LoS) link is considered, while all other possible links are neglected. To elaborate briefly on this assumption, for BSS-RIS-aided communications the typical assumption is that no LoS link is available, hence

¹Under this definition, a RIS will have an EAR 100% with threshold percentage ε when each element has a radiated power higher than ε of the average power, while a RIS will have the minimum EAR, when a single element radiates all the power.

²The multi-layer precoding design of US-RIS proposed in Section IV is unchanged even if the number of elements on each layer is different. However, it will affect the performance of communications. The discussion about the performance against the number of elements on each layer is left for future work.

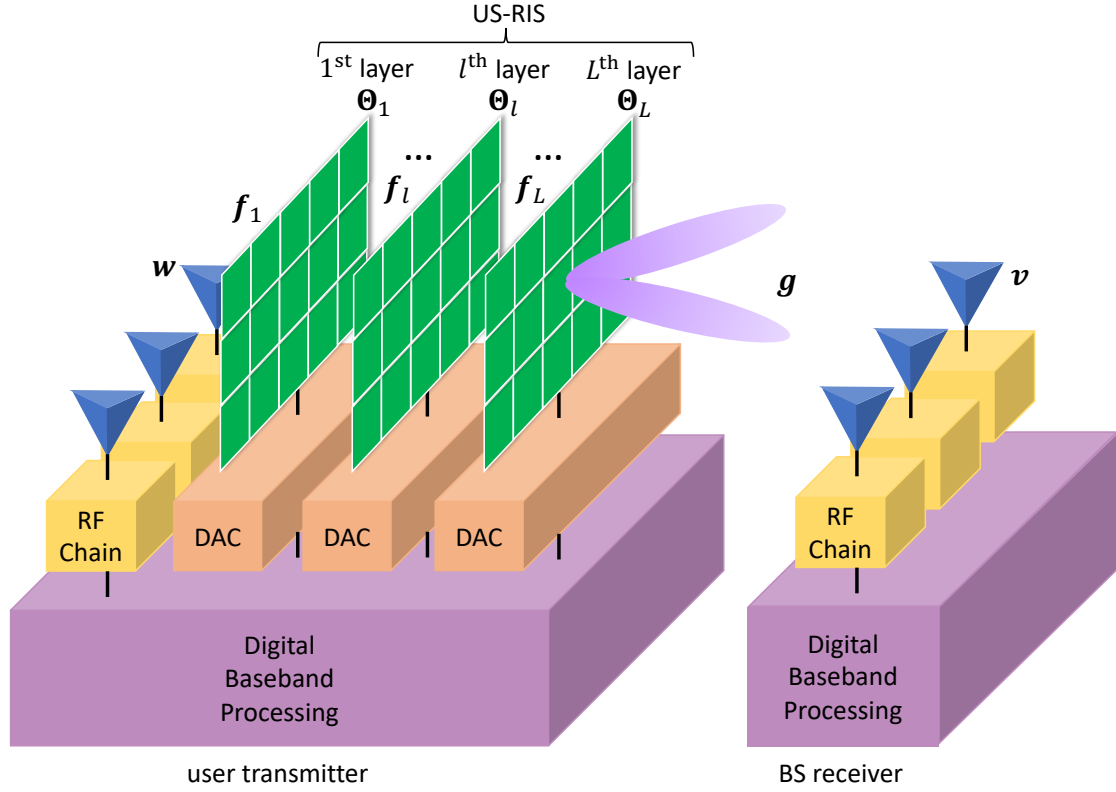


Fig. 3. System model of US-RIS-aided uplink transmission from a user to the BS, relying on the uplink transmit beamforming (UL-TBF) vector \mathbf{w} , transmit phase shifter (TPS) matrices $\Theta_1, \dots, \Theta_L$, and on the receiver combining (RC) vector \mathbf{v} communicating over the wireless channels.

the BSS-RIS directs the energy from the source to the destination. Let us denote the transmit phase shifter (TPS) matrix of US-RIS's l -th layer by

$$\Theta_l = \text{diag}(\boldsymbol{\theta}_l) = \text{diag}\left([\theta_{l,1}, \dots, \theta_{l,N}]^T\right), \quad (1)$$

where $\theta_{l,n} \in \mathcal{F}$ of Fig. 3 is the phase shift of the (l, n) -th element and \mathcal{F} is the feasible set of the transmission coefficients (TC). In this paper, we consider the widely used TC set of

$$\mathcal{F} = \left\{ \theta \mid \theta = e^{j\varphi}, \varphi \in [-\pi, \pi] \right\}, \quad (2)$$

which indicates that only the phase $\theta_{l,n}$ can be controlled independently and continuously [18]. Therefore, the signal received by the BS can be modeled as

$$\mathbf{y} = \mathbf{g}^H \left(\prod_{l=1}^L \kappa \Theta_l \mathbf{f}_l \right) \mathbf{w} s + \mathbf{n}, \quad (3)$$

where κ denotes the loss factor when the electromagnetic wave penetrates each layer. Furthermore, $\mathbf{g} \in \mathbb{C}^{N \times M}$, $\mathbf{f}_1 \in \mathbb{C}^{N \times K}$, and $\mathbf{f}_l \in \mathbb{C}^{N \times N}$ of Fig. 3 denote the frequency-domain channels

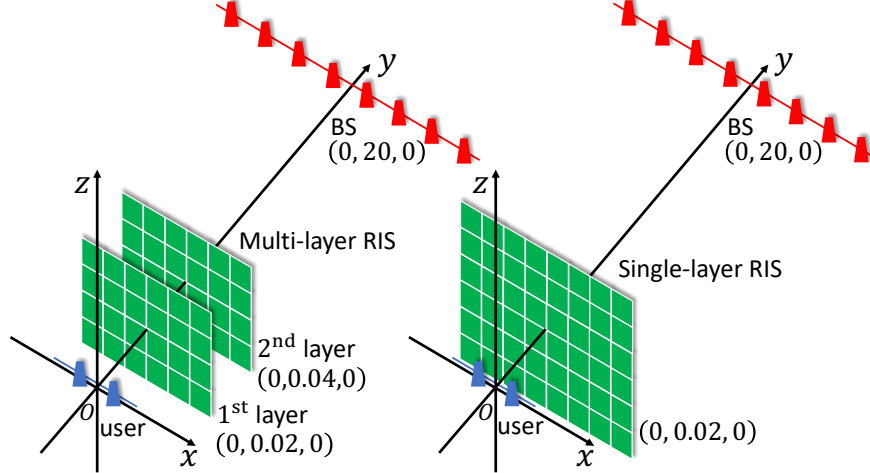


Fig. 4. A simplified system having $L = 2$ layer is employed to assist the uplink transmission from a single-antenna user. The scale is exaggerated compared to a practical system for clarity.

spanning from the US-RIS's L -th layer to the BS, from the user to the US-RIS's first layer, and from the US-RIS's $(l - 1)$ -st layer to the l -th layer, for all $l \in \{2, 3, \dots, L\}$, respectively. Still referring to (3), $\mathbf{n} \sim \mathcal{CN}(\mathbf{0}_M, \sigma^2 \mathbf{I}_M)$ denotes the additive white Gaussian noise (AWGN) introduced at the BS receiver, where σ^2 is the noise power. Finally, the BS receiver combines the signal gleaned from M antennas using a receiver combining (RC) vector $\mathbf{v} \in \mathbb{C}^{M \times 1}$ of Fig. 3. Thus, the uplink signal combined at the BS receiver can be represented as

$$z = \mathbf{v}^H \mathbf{y} = \mathbf{v}^H \mathbf{g}^H \left(\prod_{l=L}^1 \kappa \Theta_l \mathbf{f}_l \right) \mathbf{w}_S + \mathbf{v}^H \mathbf{n}. \quad (4)$$

To illustrate the benefits of the US-RIS based on this system model³, the theoretical analysis and the achievable SNR of our US-RIS-aided system will be provided in Section III and Section IV, respectively.

III. PERFORMANCE ANALYSIS

In this section, we theoretically analyze the performance of the proposed US-RIS with multi-layer structure by considering a simplified system.

Specifically, a multi-layer US-RIS having $L = 2$ layers is employed to assist the uplink transmission from a single-antenna user, as shown in Fig. 4. Let us denote the number of

³The multi-layer structure can also be applied at the BS side using a similar system model, which can also obtain the structural benefits discussed.

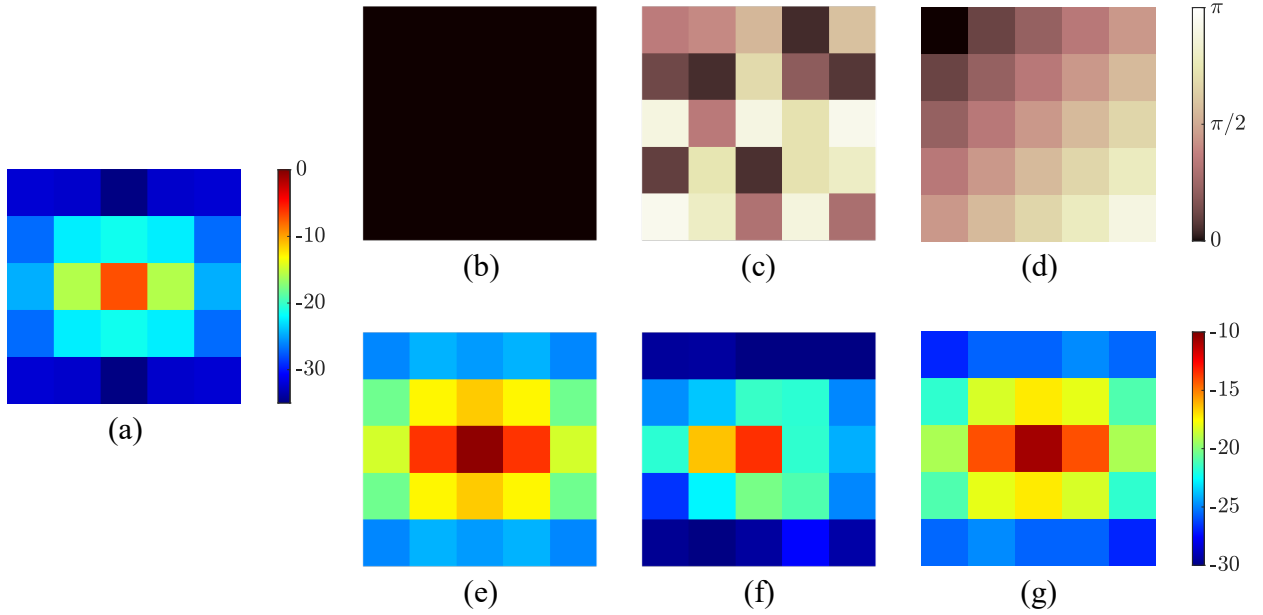


Fig. 5. An example of power distributions of the signal received on different layers for different phase-shift configurations. (a) Power distribution of the first layer (unit: dBW). (b)-(d) Three different phase shifts of the first layer of US-RIS (colorbar on the right is unified for 3 subfigures, unit: rad). (e)-(g) Power distributions of the second layer corresponding to the phase shifts displayed in (b)-(d) (colorbar on the right is unified for 3 subfigures, unit: dBW).

elements in each layer by $N = b^2$, where each element is of size $a \times a$. The position of the user is $\mathbf{s}_t = (0, 0, 0)$, and the US-RIS's two layers are positioned at the plane $y = d_1$ and $y = d_1 + d_2$ respectively, with their boundaries parallel to the coordinates and their geometric centers on the y -axis. Then, the position of each element is fixed. Specifically, for the (l, n) -th element of US-RIS, the position of the center can be written as $\mathbf{s}_r = (\alpha_n, \sum_{i=1}^l d_i, \beta_n)$, where α_n and β_n are explicit functions with respect to n . Thus, the region enclosed by the (l, n) -th element can be represented as

$$\Omega_{l,n} = \left\{ -\frac{a}{2} \leq x - \alpha_n \leq \frac{a}{2}, y = \sum_{i=1}^l d_i, -\frac{a}{2} \leq z - \beta_n \leq \frac{a}{2} \right\}. \quad (5)$$

We assume that, for single-layer RISs, only the phase shift of each element can be controlled continuously. However, for the multi-layer structure, the power distribution of the second layer can be adjusted by controlling the phase shifts on the first layer, so that the radiated power can be focused on specific elements of the second layer. This allows the amplitude of the signals penetrating multi-layer US-RISs to be controlled to some extent.

In order to understand this intuitively, a numerical example is given Fig. 5. Specifically, the power distribution of the signal received on the first layer is shown in Fig. 5 (a). Given the different phase-shift configurations on the first layer displayed in Fig. 5 (b)-(d), the patterns of power distributions on the second layer become different as shown in Fig. 5 (e)-(g), indicating that the power distribution can be controlled by multi-layer precoding. Equivalently, it can be readily seen that the amplitude term of signals penetrating the multi-layer US-RIS can be controlled to some extent, indicating that the a new DoF is brought to our US-RIS-aided transmit beamformer design⁴. This result is formally stated in **Lemma 1**.

Lemma 1 *Upon denoting the signal radiated from the $(2, n)$ -th element of the US-RIS by y_n , the phase of y_n can be adjusted to any desired angle in $[-\pi, \pi]$, while the amplitude of y_n can be adjusted in the range $[0, \zeta_n]$, where we have:*

$$\zeta_n^2 = \frac{1}{16\pi^2} \int_{-\frac{ab}{2}}^{\frac{ab}{2}} dp_x \int_{-\frac{ab}{2}}^{\frac{ab}{2}} dp_z \frac{d_1 d_2 (p_x^2 + d_1^2) ((p_x - \alpha_n)^2 + d_2^2)}{(p_x^2 + p_z^2 + d_1^2)^{5/2} ((p_x - \alpha_n)^2 + (p_z - \beta_n)^2 + d_2^2)^{5/2}}. \quad (6)$$

Proof: The proof is given in Appendix A in two steps. In particular, the closed-form expression of y_n is given in (20), and the legitimate ranges of the phase and amplitude are then discussed. ■

Remark 1 *In Lemma 1, we have stated that, for a specific n , the phase and amplitude of y_n can be controlled in a range. However, due to the coupling of $\theta_{1,1}, \dots, \theta_{1,N}$, the phases of y_1, \dots, y_N cannot be controlled independently since the amplitudes of y_1, \dots, y_N exhibit correlation. The effect of this correlation is set aside for future research.*

IV. MULTI-LAYER TRANSMIT BEAMFORMER DESIGN

To further investigate the proposed US-RIS, in this section, we extend our discussions to the more general case of $L \geq 2$ and $K \geq 1$. Based on the system model developed, we first formulate our SNR maximization problem in Subsection IV-A, which is non-convex. We will circumvent this challenge by developing a multi-layer transmit beamformer design relying on an iterative algorithm. Then, the overview of our multi-layer transmit beamformer design is provided in Subsection IV-B, while the intricate details of the optimization process are discussed in Subsection IV-C. Finally, the convergence and the computational complexity of the multi-layer transmit beamformer design are analyzed in Subsection IV-D and Subsection IV-E, respectively.

⁴This phenomenon will be quantitatively analyzed in Subsection V-D.

A. Problem formulation

Based on the system model of Fig. 3 in Section II, we aim for maximizing the detection SNR of the proposed US-RIS-aided system. Observe from the uplink signal z combined at the BS as shown in (4) that an equivalent noise contribution of $\mathbf{v}^H \mathbf{n}$ is introduced, which obeys $\mathbf{v}^H \mathbf{n} \sim \mathcal{CN}\left(0, \|\mathbf{v}^H\|_2^2 \sigma^2\right)$. Hence, the detection SNR at the BS can be represented as

$$\text{SNR} = \frac{|\mathbf{v}^H \mathbf{g}^H (\prod_{l=1}^L \kappa \Theta_l \mathbf{f}_l) \mathbf{w}|^2}{\|\mathbf{v}^H\|_2^2 \sigma^2}. \quad (7)$$

Then, given the maximum transmit power constraint of the user and phase shifts constraint at the US-RIS, the SNR maximization problem is formulated as

$$\max_{\mathbf{v}, \Theta_1, \dots, \Theta_L, \mathbf{w}} \text{SNR} = \frac{|\mathbf{v}^H \mathbf{g}^H (\prod_{l=1}^L \kappa \Theta_l \mathbf{f}_l) \mathbf{w}|^2}{\|\mathbf{v}^H\|_2^2 \sigma^2}, \quad (8a)$$

$$\text{s.t. } C_1 : \|\mathbf{w}\|_2^2 \leq P_{\max}, \quad (8b)$$

$$C_2 : |\theta_{l,n}| = 1, \forall l, n. \quad (8c)$$

Due to the non-convexity of the objective function (8a) and the constraint (8c), the joint optimization of both the RC vector \mathbf{v} , as well as of the US-RIS TPS matrices $\Theta_1, \dots, \Theta_L$, and of the UL-TBF vector \mathbf{w} is challenging. To tackle this challenge, we propose an iterative algorithm as our multi-layer transmit beamformer design.

B. Overview of the proposed multi-layer transmit beamformer design

The algorithm of solving this joint optimization problem (8) is summarized in **Algorithm 1**. Specifically, given the input channel matrices and parameters, the coupled variables $\mathbf{v}, \Theta_1, \dots, \Theta_L$, and \mathbf{w} can be optimized by alternately updating one variable with the other variables fixed. Once convergence of the objective function is reached, the iterations are curtailed, and the optimal beamformer design is found.

C. Optimal UL-TBF, TPS, and RC of Fig. 3

In this subsection, we derive the closed-form expression of the optimal solution corresponding to each variable. For ease of notation, we first define

$$\xi_{(p,q)} = \begin{cases} \prod_{l=p}^q \kappa \Theta_l \mathbf{f}_l, & p \in [L], q \in [L], \\ \mathbf{I}_N, & p = L, q = L + 1, \\ \mathbf{I}_K, & p = 0, q = 1. \end{cases} \quad (9)$$

Algorithm 1 Multi-layer transmit beamformer design for US-RIS-aided communications

Input: Channel matrices $\mathbf{f}_1, \dots, \mathbf{f}_L$, and \mathbf{g} ; maximum transmit power P_{\max} .

Output: Optimized RC vector \mathbf{v} ; optimized US-RIS TPS matrices $\Theta_1, \dots, \Theta_L$; optimized UL-TBF vector \mathbf{w} ; maximized SNR.

- 1: Initialize $\mathbf{v}, \Theta_1, \dots, \Theta_L$, and \mathbf{w} ;
 - 2: **while** no convergence of SNR **do**
 - 3: Update \mathbf{v}^{opt} by (11);
 - 4: Update $\Theta_1^{\text{opt}}, \dots, \Theta_L^{\text{opt}}$ in turn by (14);
 - 5: Update \mathbf{w}^{opt} by (17);
 - 6: Update SNR by (7);
 - 7: **end while**
 - 8: **return** $\mathbf{v}, \Theta_1, \dots, \Theta_L, \mathbf{w}$, and SNR.
-

Then, the updates of different variables are respectively provided as follows.

1) *Optimal RC*: For determining the RC vector \mathbf{v} of Fig. 3, while fixing all the other variables, the optimization problem (8) can be equivalently reformulated as

$$\max_{\mathbf{v}} \text{SNR} = \frac{\mathbf{v}^H \mathbf{g}^H \boldsymbol{\xi}_{(L,1)} \mathbf{w} \mathbf{w}^H \boldsymbol{\xi}_{(L,1)}^H \mathbf{g} \mathbf{v}}{\|\mathbf{v}^H\|_2^2 \sigma^2} := \frac{\mathbf{v}^H \mathbf{U} \mathbf{v}}{\|\mathbf{v}^H\|_2^2 \sigma^2}, \quad (10)$$

where $\mathbf{U} = \mathbf{g}^H \boldsymbol{\xi}_{(L,1)} \mathbf{w} \mathbf{w}^H \boldsymbol{\xi}_{(L,1)}^H \mathbf{g}$ is a positive semidefinite matrix. Based on matrix analysis, the maximum SNR can be achieved when \mathbf{v} is the eigenvector of \mathbf{U} , corresponding to its largest eigenvalue, which is formulated as

$$\mathbf{v}^{\text{opt}} = \psi_{\max} (\mathbf{g}^H \boldsymbol{\xi}_{(L,1)} \mathbf{w} \mathbf{w}^H \boldsymbol{\xi}_{(L,1)}^H \mathbf{g}). \quad (11)$$

2) *Optimal US-RIS TPS*: For the TPS matrix Θ_l ($l \in [L]$), since $\Theta_l \equiv \text{diag}(\boldsymbol{\theta}_l)$ is a diagonal matrix and $\mathbf{f}_l \boldsymbol{\xi}_{(l-1,1)} \mathbf{w}$ is a column vector, we have

$$\boldsymbol{\xi}_{(l,1)} \mathbf{w} = \text{diag}(\mathbf{f}_l \boldsymbol{\xi}_{(l-1,1)} \mathbf{w}) \boldsymbol{\theta}_l. \quad (12)$$

By exploiting the transformation (12), the SNR can be rewritten as

$$\text{SNR} = \frac{|\mathbf{v}^H \mathbf{g}^H \boldsymbol{\xi}_{(L,1)} \mathbf{w}|^2}{\|\mathbf{v}^H\|_2^2 \sigma^2} = \frac{|\mathbf{v}^H \mathbf{g}^H \boldsymbol{\xi}_{(L,l+1)} \boldsymbol{\xi}_{(l,1)} \mathbf{w}|^2}{\|\mathbf{v}^H\|_2^2 \sigma^2} = \frac{|\mathbf{v}^H \mathbf{g}^H \boldsymbol{\xi}_{(L,l+1)} \text{diag}(\mathbf{f}_l \boldsymbol{\xi}_{(l-1,1)} \mathbf{w}) \boldsymbol{\theta}_l|^2}{\|\mathbf{v}^H\|_2^2 \sigma^2}. \quad (13)$$

Because of the constraint (8c), the optimal value of θ_l is obtained when all entries of θ_l have the complementary phase angle as the vector multiplied on the left, which is expressed as

$$\theta_l^{\text{opt}} = \exp \left(j \arg \left(\text{diag} \left(\mathbf{f}_l \boldsymbol{\xi}_{(l-1,1)} \mathbf{w} \right)^H \boldsymbol{\xi}_{(L,l+1)}^H \mathbf{g} \mathbf{v} \right) \right), \quad \forall l \in [L]. \quad (14)$$

3) *Optimal UL-TBF*: Finally, for the UL-TBF vector \mathbf{w} , we first consider the optimization of the normalized vector $\langle \mathbf{w} \rangle$, i.e.,

$$\begin{aligned} \max_{\langle \mathbf{w} \rangle} \frac{|\mathbf{v}^H \mathbf{g}^H \boldsymbol{\xi}_{(L,1)} \langle \mathbf{w} \rangle|^2}{\|\mathbf{v}^H\|_2^2 \sigma^2} &= \frac{\text{SNR}}{\|\mathbf{w}\|_2^2}, \\ \text{s.t. } \|\langle \mathbf{w} \rangle\|_2 &= 1. \end{aligned} \quad (15)$$

We then obtain the optimized $\langle \mathbf{w} \rangle$ as

$$\langle \mathbf{w} \rangle^{\text{opt}} = \langle \boldsymbol{\xi}_{(L,1)}^H \mathbf{g} \mathbf{v} \rangle. \quad (16)$$

Upon considering the constraint (8b) and the relationship between the optimized \mathbf{w} for the subproblem (8) and the optimized $\langle \mathbf{w} \rangle$ for the subproblem (15), we arrive at

$$\mathbf{w}^{\text{opt}} = \sqrt{P_{\max}} \langle \mathbf{w} \rangle^{\text{opt}} = \sqrt{P_{\max}} \langle \boldsymbol{\xi}_{(L,1)}^H \mathbf{g} \mathbf{v} \rangle. \quad (17)$$

D. Convergence analysis

For the proposed multi-layer transmit beamformer design, we adopt the general assumption that only the phase shifts of the elements can be continuously controlled. Under this assumption, if the variables are alternately updated according to (11), (14), and (17), which is the optimal solution of the corresponding subproblem with all the other variables fixed, the objective function, namely the SNR, will increase monotonically, hence indicating the strict convergence of the multi-layer transmit beamformer design.

E. Complexity analysis

The overall computational complexity of the proposed multi-layer transmit beamformer design is dominated by the updates of the variables \mathbf{v} , $\Theta_1, \dots, \Theta_L$, and \mathbf{w} , as shown in (11), (14), and (17), respectively. Note however that, the $\boldsymbol{\xi}_{(p,q)}$ terms associated with different p and q have strong correlation that may be exploited for reducing the redundancy of the repeated matrix multiplications. Specifically, all $\boldsymbol{\xi}_{(p,q)}$ terms involved in (11), (14), and (17) can be obtained throughout the computational processes of $\boldsymbol{\xi}_{(L,1)}$ and $\boldsymbol{\xi}_{(L,2)}$, hence only the computational complexities of $\boldsymbol{\xi}_{(L,1)}$ and $\boldsymbol{\xi}_{(L,2)}$ actually count in the $\boldsymbol{\xi}_{(p,q)}$ terms of the parameter updates.

TABLE II
COMPLEXITY OF UPDATING EACH VARIABLE

| Variable | Complexity $\mathcal{O}(\cdot)$ |
|-------------------------------------------------------|---------------------------------|
| $\xi_{(L,1)}$ | $LNK + (L - 1)N^2K$ |
| $\xi_{(L,2)}$ | $(L - 1)N^2 + (L - 2)N^3$ |
| \mathbf{v}^{opt} | $NK + MN + M^2$ |
| $\Theta_1^{\text{opt}}, \dots, \Theta_L^{\text{opt}}$ | $L(NK + N^2K + MN + N^2)$ |
| \mathbf{w}^{opt} | $MN + MNK + K$ |

We have summarized the computational complexities of the variables in TABLE II. Since the number of RIS elements is usually high [22], we can reasonably assume that $N \gg K$ and $N^2 \gg M$. Furthermore, due to the loss factor characterizing the process when the electromagnetic waves penetrate each layer, the number of layers L must not be large compared to N , i.e. we have $N \gg L$. Under these assumptions, the overall complexity of the proposed multi-layer precoding design in a single iteration may be approximated by $\mathcal{O}(N^3 + MNK + M^2)$. For comparison, the complexity analysis of the beamformer design in BSS-RIS-aided communications can be regarded as a special case of the US-RIS-aided scenario, where the BSS-RIS has a single-layer structure associated with LN elements, which is the same as the total number of elements in our US-RIS. Therefore, the complexity of a single iteration in the multi-layer transmit beamformer design of BSS-RIS-aided communications is $\mathcal{O}(N^3L^3 + MNKL + M^2)$. Since we have $N \gg L$, the computational complexity of the proposed multi-layer transmit beamformer design is almost the same as that of the traditional BSS-RIS-aided communications, which is affordable in practice.

V. SIMULATION RESULTS

In this section, we provide extensive simulation results for quantifying the performance of the proposed US-RIS concept and of the corresponding multi-layer transmit beamformer design for US-RIS-aided communications. The simulation scenario is introduced first in Subsection V-A. Then, numerical results are discussed in the following subsections.

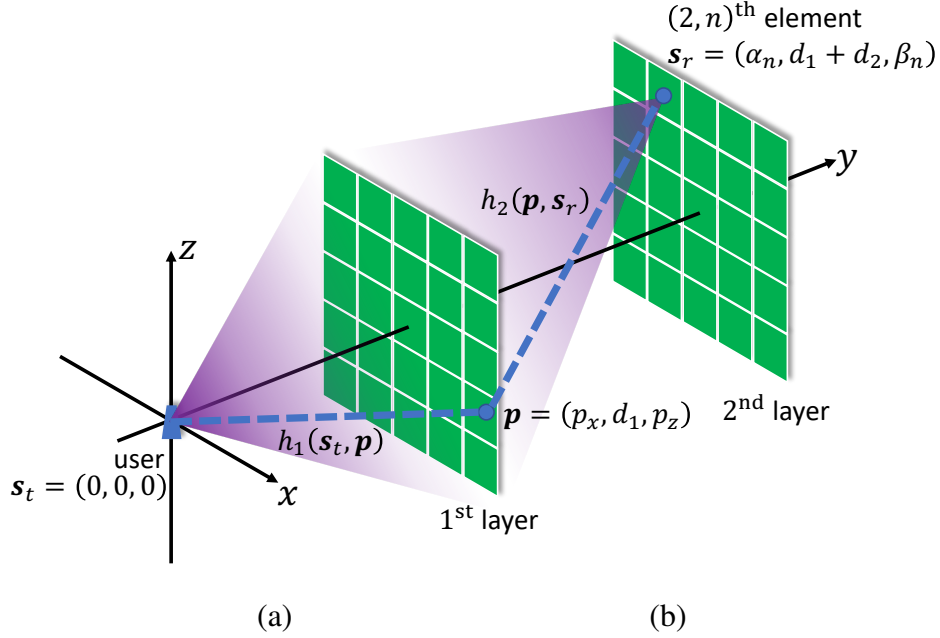


Fig. 6. The simulation scenario where different types of RISs are employed to assist communications. (a) Multi-layer US-RIS-aided communications. (b) Single-layer US/BSS-RIS-aided communications.

A. Simulation setup

For simplicity but without loss of generality, we consider a 3-D scenario where different types of RISs are employed for uplink transmission from the user to the BS. Specifically, the topology considered is shown in Fig. 6. Let λ denote the wavelength of the transmitted uplink signal. We assume that both the user and the BS are equipped with a uniform linear array (ULA) having 2 and 8 antennas, respectively, where the distance between the adjacent elements is $\frac{\lambda}{2}$ [23]. A multi-layer US-RIS, with 2 layers and 8×12 elements on each layer, is used for enhancing the user's uplink transmission, as shown in Fig. 6 (a). For comparison, we consider another two cases, where a single-layer US-RIS and a single-layer reflective BSS-RIS having 12×16 elements are respectively used at the same position as the multi-layer US-RIS's first layer shown in Fig. 6 (b). The total number of elements in the multi-layer US-RIS, single-layer US-RIS, and single-layer BSS-RIS are the same, and they are all uniform planar arrays (UPAs), where the elements of size $\frac{\lambda}{2} \times \frac{\lambda}{2}$ are closely packed with no spacing [24]. We assume that the user, the multi-layer US-RIS's first layer (located at the same position as the single-layer US/BSS-RIS), the multi-layer US-RIS's second layer, and the BS are located with their centers at $(0 \text{ m}, 0 \text{ m}, 0 \text{ m})$, $(0 \text{ m}, 0.02 \text{ m}, 0 \text{ m})$, $(0 \text{ m}, 0.04 \text{ m}, 0 \text{ m})$, and $(0 \text{ m}, 20 \text{ m}, 0 \text{ m})$, respectively. The frequency of the

transmitted signal is set to $f = 2.5\text{ GHz}$. The noise power is set to $\sigma^2 = 1 \times 10^{-6}$. The loss factor κ when a wave penetrates a transmissive RIS is set to 0.8.

As for the channel model, we categorize all channels involved into two types. The RIS-BS channel is the Type I channel which is a far-field channel assumed to obey the free-space propagation, where an ideal transmit antenna sends a signal to a lossless receive antenna. The pathloss of the Type I channel can be directly obtained from Friis' formula [25]. On the other hand, the user-RIS and RIS-RIS channels are termed as the Type II channels. To elaborate, the Type II channel is the near-field channel that is considered as the channel spanning from a lossless antenna to an element of the UPA under the LoS assumption. The lossless transmit antenna can be either an element of a ULA or an element of a UPA, corresponding to the user-RIS and RIS-RIS channels. For the pathloss of the Type II channel, we adopt the exact expression introduced in [26]. Note that, the other potential links are ignored, as mentioned in Section II.

Finally, we assume for the proposed multi-layer transmit beamformer design that the channel state information (CSI) is perfectly known [15], [27], which can be estimated through RIS-based channel estimation and channel feedback methods in practice [28]–[30]. Specifically, in US-RIS-aided communications, the channel spanning from the user to the US-RIS and that between adjacent layers of the US-RIS can be estimated beforehand, thanks to stability ensured by the enclosure. As for the initializations, all RISs are initialized by random phase values in the feasible set, while the UL-TBF and RC vectors are initialized as ones in our iterative algorithm.

B. Performance of the US-RIS-aided communications

In Fig. 7, we portray the detection SNR versus the maximum transmit power P_{\max} for different RIS scenarios. We also consider a “*No RIS*” benchmark for comparison [15], where the RIS shown in Fig. 6 is removed but the optimization of UL-TBF vector and RC vector based on the Type I UE-BS channel is retained.

Observe from Fig. 7 that the SNR versus the maximum transmit power P_{\max} exhibits a near-linear relationship, which can also be observed from the parameter updates (11), (14), and (17). Therefore, we can readily compare different scenarios with the power constraint P_{\max} fixed. The associated differences are marked in Fig. 7. Observe that the communication without RISs has the lowest SNR, illustrating that all three RIS scenarios can substantially improve the uplink transmission. Another observation is that the single-layer US-RIS-aided communications has a

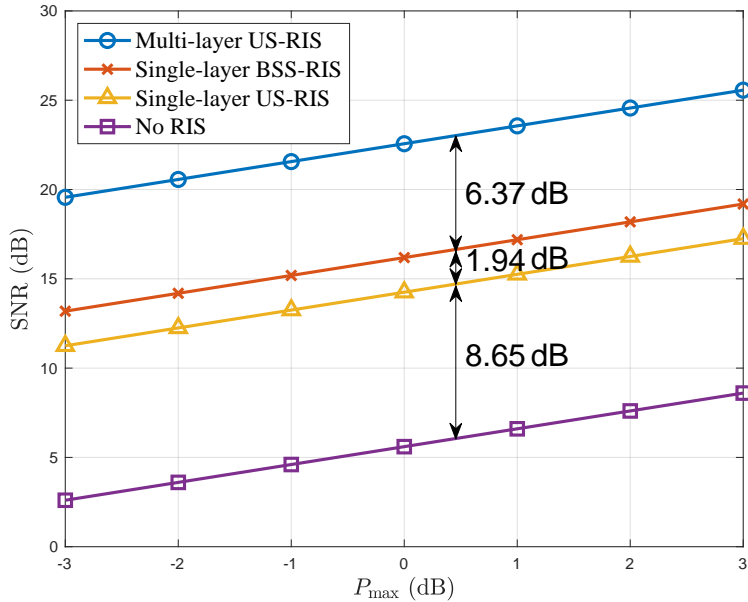


Fig. 7. Detection SNR versus the maximum transmit power P_{\max} .

1.94 dB loss compared to its single-layer BSS-RIS-aided counterpart, which is caused by the loss when a wave penetrates the RIS. Moreover, the multi-layer US-RIS-aided communications has a 6.37 dB SNR over its single-layer BSS-RIS-aided counterpart for the same total number of RIS elements, which is an explicit benefit of its increased DoF of the transmitted beam, compared to the conventional single-layer structure.

For further characterizing the multi-layer structure, in Fig. 8 we present the radiation pattern of different RISs and compare the quality of the beam by comparing their mainlobes and sidelobes. Naturally, a beam having lower sidelobes and a higher mainlobe is preferred. Observe from Fig. 8 that the transmitted beam of the first layer in the multi-layer US-RIS has a lower mainlobe than the single-layer US-RIS, which is caused by the reduced number of elements in the first layer of the multi-layer US-RIS. However, after penetrating the second layer and obtaining a new DoF in amplitude terms, the mainlobe to sidelobe ratio is considerably improved. The above results coincide well with our theoretical analysis provided in Section III.

C. Convergence of the proposed multi-layer transmit beamformer design

Recall from Subsection IV-D that, the proposed multi-layer transmit beamformer design exhibits monotonic convergence. In Fig. 9, we further characterize its convergence in the simulation scenario considered. The results of Fig. 9 clearly illustrate that, the proposed multi-layer

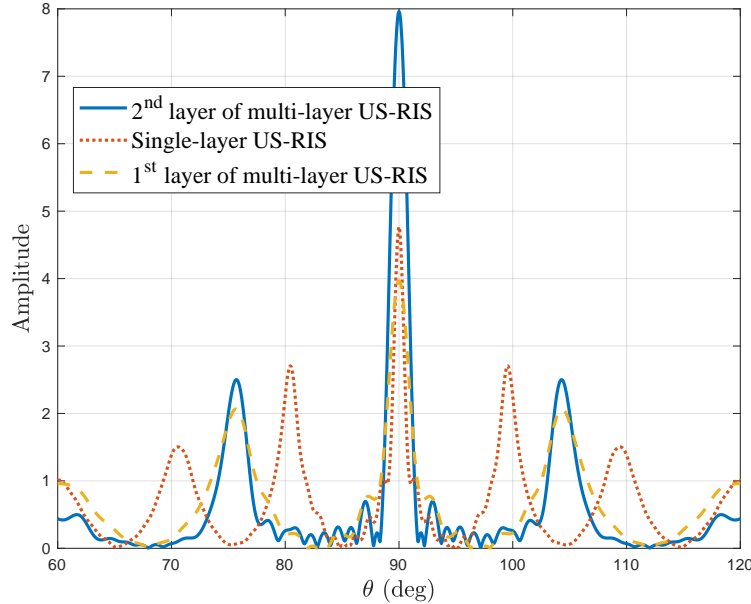


Fig. 8. Radiation pattern of different RISs.

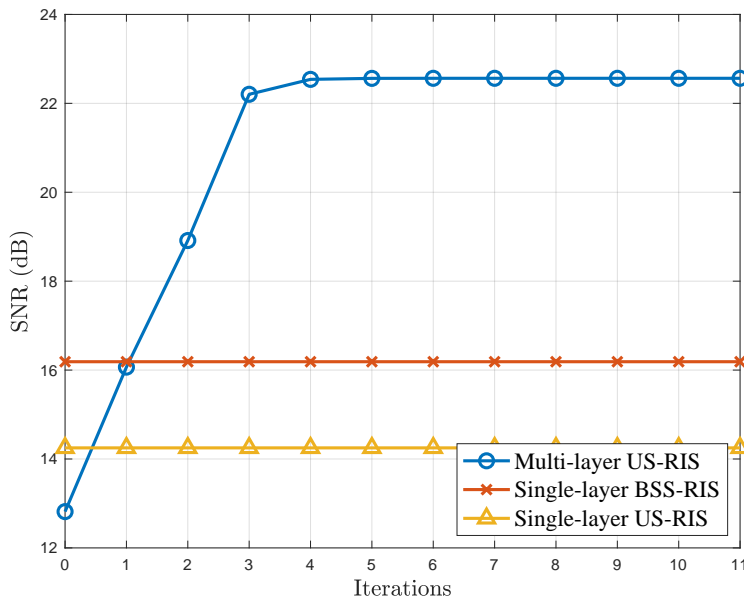


Fig. 9. Detection SNR at $P_{\max} = 0$ dBW against the number of iterations.

transmit beamformer design for multi-layer US-RIS converges within 4 to 5 iterations, while the conventional single-layer BSS-RIS-aided scheme converges within 1 to 2 iterations. However, our solution outperforms the latter after the first iteration.

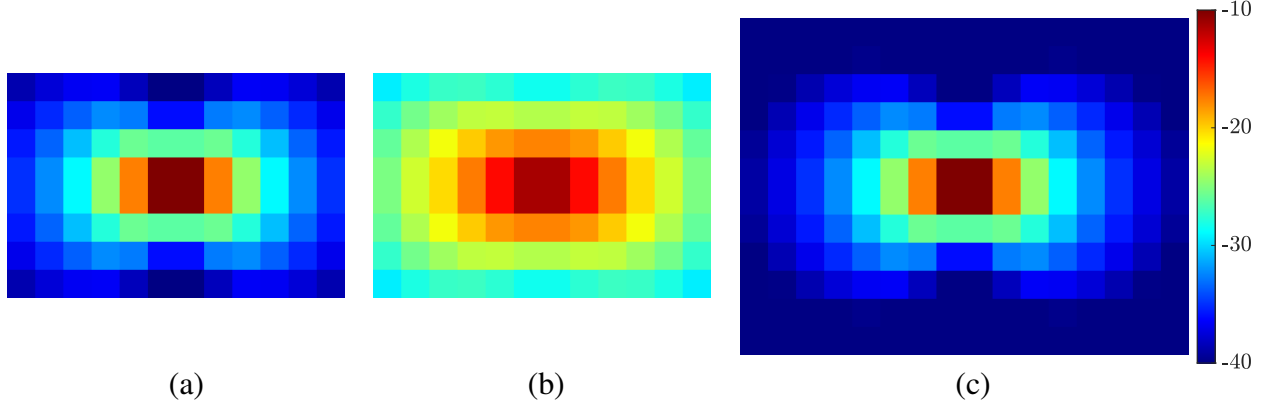


Fig. 10. Power distribution of multi-layer and single-layer US-RIS (colorbar on the right is unified for 3 subfigures, unit: dBW), implying different EARs of different RISs. Threshold percentage is set to $\varepsilon = 1/6$. (a) The first layer of multi-layer US-RIS with EAR 29.2%. (b) The second layer of multi-layer US-RIS with EAR 87.5%. (c) Single-layer US-RIS with EAR 22.9%.

D. EAR Analysis on RIS

To further reveal the benefits of the multi-layer structure in controlling the amplitude of the signal, the power distribution of both multi-layer and single-layer US-RIS are presented in Fig. 10. Observe from Fig. 10 (a) and (c) that both in the first layer of the multi-layer US-RIS and in the single-layer US-RIS, the central elements are assigned most of the power, while the non-central elements have a limited contribution. By contrast, as shown in Fig. 10 (b), the power distribution is transformed to a more balanced power pattern in the second layer of US-RIS with the aid of the phase shift control of the first layer. Although the power of the central elements is reduced, the elements along the edges become more influential.

To quantify this phenomenon, we apply the EAR metric defined in Subsection II-B. Explicitly, the EARs of different RISs with a threshold percentage $\varepsilon = 1/6$ are shown in Fig. 10. The first layer of the multi-layer US-RIS has an EAR of 29.2%, which is higher than that of the single-layer US-RIS having an EAR of 22.9%, because the first layer of the multi-layer US-RIS has fewer elements. Furthermore, as a benefit of the multi-layer structure, the EAR of the second layer of the US-RIS is 87.5%, and the overall EAR of the multi-layer US-RIS is 58.3%, which is twice higher than that of the single-layer US-RIS. The obvious improvement in EAR also demonstrates the ascendancy of the proposed architecture with multi-layer structure.

VI. SUMMARY AND CONCLUSIONS

In this paper, we have proposed the concept of US-RIS to circumvent the space-limit of employing a large-scale array at the user side. In contrast to the existing BSS-RISs, we have proposed a solution that is suitable for the user side. Based on this concept, we have further proposed a novel architecture with the aid of a multi-layer US-RIS. Our theoretical analysis has demonstrated that the amplitude of the signal penetrating the multi-layer US-RIS can also be partially controlled, which equips us with a new DoF. Furthermore, we have formulated the associated SNR maximization problem in the US-RIS-aided communications and have proposed the corresponding multi-layer transmit beamformer design that alternately finds the optimal solution for each variable. Our simulation results have verified the superiority of the proposed multi-layer US-RIS as a realization of a large-scale array at the user side for uplink transmission.

However, a whole spate of open problems associated with multi-layer US-RIS requires further investigations in our future work. For example, the theoretical analysis of this appealing multi-layer structure is based on the assumption that the RIS phase shifts can be controlled continuously, while in practice only discrete phase shifts can be realized [31]. Furthermore, the RIS-element correlation has been neglected in this study, which requires special attention. Finally, diverse propagation scenarios have to be considered.

APPENDIX A PROOF OF LEMMA 1

Following the notations in Section III, the proof proceeds in two steps. In the first step, we derive the closed-form expression of y_n by integration. In the second step, under the assumption of controllable US-RIS phase shift matrices, we analyze the range of phase and amplitude of y_n , respectively.

A. Closed-form expression of y_n

Denote the channel spanning from the point source s_t at the user to the arbitrary receiver point $\mathbf{p} = (p_x, d_1, p_z)$ on the US-RIS's first layer and the channel spanning from \mathbf{p} to the center

of the $(2, n)$ -th element by $h_1(\mathbf{s}_t, \mathbf{p})$ and $h_2(\mathbf{p}, \mathbf{s}_r)$, respectively. The expression of $h_1(\mathbf{s}_t, \mathbf{p})$ and $h_2(\mathbf{p}, \mathbf{s}_r)$ can be written as

$$h_1(\mathbf{s}_t, \mathbf{p}) = |h_1(\mathbf{s}_t, \mathbf{p})| \exp\left(-j \frac{2\pi}{\lambda} \|\mathbf{p} - \mathbf{s}_t\|\right), \quad (18a)$$

$$h_2(\mathbf{p}, \mathbf{s}_r) = |h_2(\mathbf{p}, \mathbf{s}_r)| \exp\left(-j \frac{2\pi}{\lambda} \|\mathbf{s}_r - \mathbf{p}\|\right), \quad (18b)$$

where λ denotes the wavelength and

$$|h_1(\mathbf{s}_t, \mathbf{p})|^2 = \frac{1}{4\pi} \frac{d_1(p_x^2 + d_1^2)}{(p_x^2 + p_z^2 + d_1^2)^{5/2}}, \quad (19a)$$

$$|h_2(\mathbf{p}, \mathbf{s}_r)|^2 = \frac{1}{4\pi} \frac{d_2((p_x - \alpha_n)^2 + d_2^2)}{((p_x - \alpha_n)^2 + (p_z - \beta_n)^2 + d_2^2)^{5/2}}, \quad (19b)$$

represent the channel gain along the y -direction, respectively [26], [32]. Upon integrating over all receive points on the US-RIS's first layer and considering the phase shift $\theta_{2,n}$ of the $(2, n)$ -th element, we arrive at the closed-form expression of

$$y_n = \theta_{2,n} \sum_{j=1}^N \iint_{\Omega_{1,j}} h_1(\mathbf{s}_t, \mathbf{p}) \theta_{1,j} h_2(\mathbf{p}, \mathbf{s}_r) d\mathbf{p}. \quad (20)$$

B. Range of phase and amplitude

As for the range of the phase $\arg(y_n)$, recall from (20) that, since the phase of $\theta_{2,n}$ can be controlled continuously in $[-\pi, \pi]$, the phase of y_n can also be controlled continuously in $[-\pi, \pi]$.

As for the range of amplitudes $|y_n|$, we discuss the control strategy of RIS required for achieving the minimum of 0 and the maximum of ζ_n , respectively. Note that the phase shift matrix Θ_2 does not influence the amplitude of y_n , hence we can focus our attention on the phase shift matrix Θ_1 .

To obtain the maximum amplitude, we have from (20) that

$$|y_n|^2 \leq \sum_{j=1}^N \iint_{\Omega_{1,j}} |h_1(\mathbf{s}_t, \mathbf{p}) h_2(\mathbf{p}, \mathbf{s}_r)|^2 d\mathbf{p} = \int_{-\frac{ab}{2}}^{\frac{ab}{2}} \int_{-\frac{ab}{2}}^{\frac{ab}{2}} |h_1(\mathbf{s}_t, \mathbf{p})|^2 |h_2(\mathbf{p}, \mathbf{s}_r)|^2 dp_x dp_z. \quad (21)$$

Upon substituting (18), we obtain (6).

On the other hand, to obtain the minimum amplitude, we construct a phase matrix Θ_1 that results in $y_n = 0$. A potential construction method is constituted by the following. We define the four symmetric elements centered at

$$\mathbf{s}_{r,1} = (\alpha_n, d_1 + d_2, \beta_n), \quad \mathbf{s}_{r,2} = (-\alpha_n, d_1 + d_2, \beta_n),$$

$$\mathbf{s}_{r,3} = (\alpha_n, d_1 + d_2, -\beta_n), \quad \mathbf{s}_{r,4} = (-\alpha_n, d_1 + d_2, -\beta_n),$$

as a quaternion $\mathcal{S}_n = (\mathbf{s}_{r,1}, \mathbf{s}_{r,2}, \mathbf{s}_{r,3}, \mathbf{s}_{r,4})$. The N elements on the first layer can then be divided into $\frac{N}{4}$ quaternions that do not have intersection with each other. We will show that, for each quaternion \mathcal{S}_n , there exist $\theta_1, \theta_2, \theta_3, \theta_4$ values which satisfy

$$\sum_{j=1}^4 \theta_j \iint_{\Omega_{1,j}} h_1(\mathbf{s}_t, \mathbf{p}) h_2(\mathbf{p}, \mathbf{s}_{r,j}) d\mathbf{p} = 0. \quad (22)$$

Then, for each quaternion, we can construct a group of phase shifts $\theta_1, \theta_2, \theta_3, \theta_4$, which has no contribution to y_n in (20). With the aid of this process, we obtain a solution of Θ_1 that satisfies $y_n = 0$.

In fact, based on the geometric properties, the amplitudes of the four double integral terms in (22) may form a closed quadrilateral. Hence there exist θ_j ($j \in [4]$), with $|\theta_j| = 1$, that satisfy (22).

ACKNOWLEDGMENTS

We would like to thank Richard MacKenzie from BT Group plc and Mo Hao from Tsinghua SEM Advanced ICT LAB for their discussion and support of this work.

REFERENCES

- [1] M. Giordani, M. Polese, M. Mezzavilla, S. Rangan, and M. Zorzi, “Toward 6G networks: Use cases and technologies,” *IEEE Commun. Mag.*, vol. 58, no. 3, pp. 55–61, Mar. 2020.
- [2] F. Rusek, D. Persson, B. K. Lau, E. G. Larsson, T. L. Marzetta, O. Edfors, and F. Tufvesson, “Scaling up MIMO: Opportunities and challenges with very large arrays,” *IEEE Signal Process. Mag.*, vol. 30, no. 1, pp. 40–60, Jan. 2013.
- [3] T. L. Marzetta, “Noncooperative cellular wireless with unlimited numbers of base station antennas,” *IEEE Trans. Wireless Commun.*, vol. 9, no. 11, pp. 3590–3600, Nov. 2010.
- [4] O. El Ayach, S. Rajagopal, S. Abu-Surra, Z. Pi, and R. W. Heath, “Spatially sparse precoding in millimeter wave MIMO systems,” *IEEE Trans. Wireless Commun.*, vol. 13, no. 3, pp. 1499–1513, Mar. 2014.
- [5] K. B. Letaief, W. Chen, Y. Shi, J. Zhang, and Y.-J. A. Zhang, “The roadmap to 6G: AI empowered wireless networks,” *IEEE Commun. Mag.*, vol. 57, no. 8, pp. 84–90, Aug. 2019.
- [6] S. Hu, F. Rusek, and O. Edfors, “Beyond massive MIMO: The potential of data transmission with large intelligent surfaces,” *IEEE Trans. Signal Process.*, vol. 66, no. 10, pp. 2746–2758, Oct. 2018.
- [7] C. Pan, H. Ren, K. Wang, J. F. Kolb, M. Elkashlan, M. Chen, M. Di Renzo, Y. Hao, J. Wang, A. L. Swindlehurst, X. You, and L. Hanzo, “Reconfigurable intelligent surfaces for 6G systems: Principles, applications, and research directions,” *IEEE Commun. Mag.*, vol. 59, no. 6, pp. 14–20, 2021.
- [8] E. Basar, M. Di Renzo, J. De Rosny, M. Debbah, M.-S. Alouini, and R. Zhang, “Wireless communications through reconfigurable intelligent surfaces,” *IEEE Access*, vol. 7, pp. 116 753–116 773, Aug. 2019.
- [9] Y. Liu, X. Mu, J. Xu, R. Schober, Y. Hao, H. V. Poor, and L. Hanzo, “STAR: Simultaneous transmission and reflection for 360° coverage by intelligent surfaces,” *arXiv preprint arXiv:2103.09104*, Mar. 2021.

- [10] C. Liaskos, A. Tsoliaridou, A. Pitsillides, S. Ioannidis, and I. Akyildiz, "Using any surface to realize a new paradigm for wireless communications," *Commun. ACM*, vol. 61, no. 11, pp. 30–33, Nov. 2018.
- [11] T. Bai, C. Pan, Y. Deng, M. Elkashlan, A. Nallanathan, and L. Hanzo, "Latency minimization for intelligent reflecting surface aided mobile edge computing," *IEEE J. Sel. Areas Commun.*, vol. 38, no. 11, pp. 2666–2682, Nov. 2020.
- [12] L. Dai, B. Wang, M. Wang, X. Yang, J. Tan, S. Bi, S. Xu, F. Yang, Z. Chen, M. Di Renzo, C.-B. Chae, and L. Hanzo, "Reconfigurable intelligent surface-based wireless communications: Antenna design, prototyping, and experimental results," *IEEE Access*, vol. 8, pp. 45 913–45 923, Mar. 2020.
- [13] W. Tang, X. Li, J. Y. Dai, S. Jin, Y. Zeng, Q. Cheng, and T. J. Cui, "Wireless communications with programmable metasurface: Transceiver design and experimental results," *China Commun.*, vol. 16, no. 5, pp. 46–61, Jun. 2019.
- [14] Y. Liang, R. Long, Q. Zhang, J. Chen, H. V. Cheng, and H. Guo, "Large intelligent surface/antennas (LISA): Making reflective radios smart," *J. Commun. Inf. Networks*, vol. 4, no. 2, pp. 40–50, Jun. 2019.
- [15] Z. Zhang and L. Dai, "A joint precoding framework for wideband reconfigurable intelligent surface-aided cell-free network," *IEEE Trans. Signal Process. (early access article)*, Jun. 2021.
- [16] K. Liu and Z. Zhang, "On the energy-efficiency fairness of reconfigurable intelligent surface-aided cell-free network," in *Proc. 2021 IEEE 93rd Veh. Technol. Conf. (IEEE VTC'21 Spring)*, 2021, pp. 1–6.
- [17] C. Huang, A. Zappone, G. C. Alexandropoulos, M. Debbah, and C. Yuen, "Reconfigurable intelligent surfaces for energy efficiency in wireless communication," *IEEE Trans. Wireless Commun.*, vol. 18, no. 8, pp. 4157–4170, Aug. 2019.
- [18] Q. Wu and R. Zhang, "Intelligent reflecting surface enhanced wireless network via joint active and passive beamforming," *IEEE Trans. Wireless Commun.*, vol. 18, no. 11, pp. 5394–5409, Aug. 2019.
- [19] Y. Lu and L. Dai, "Reconfigurable intelligent surface based hybrid precoding for THz communications," *arXiv preprint arXiv:2012.06261*, Dec. 2020.
- [20] Z. Yang, W. Xu, C. Huang, J. Shi, and M. Shikh-Bahaei, "Beamforming design for multiuser transmission through reconfigurable intelligent surface," *IEEE Trans. Commun.*, vol. 69, no. 1, pp. 589–601, Jan. 2021.
- [21] S. Zeng, H. Zhang, B. Di, Y. Tan, Z. Han, H. V. Poor, and L. Song, "Reconfigurable intelligent surfaces in 6G: Reflective, transmissive, or both?" *IEEE Commun. Lett. (early access article)*, Feb. 2021.
- [22] P. Wang, J. Fang, X. Yuan, Z. Chen, and H. Li, "Intelligent reflecting surface-assisted millimeter wave communications: Joint active and passive precoding design," *IEEE Trans. Veh. Technol.*, vol. 69, no. 12, pp. 14 960–14 973, Dec. 2020.
- [23] W. C. Lee, *Wireless and cellular communications*. McGraw-Hill Education, 2006.
- [24] E. Björnson, L. Sanguinetti, H. Wymeersch, J. Hoydis, and T. L. Marzetta, "Massive MIMO is a reality—What is next?: Five promising research directions for antenna arrays," *Digital Signal Processing*, vol. 94, pp. 3–20, 2019.
- [25] H. T. Friis, "A note on a simple transmission formula," *IRE*, vol. 34, no. 5, pp. 254–256, May 1946.
- [26] E. Björnson and L. Sanguinetti, "Power scaling laws and near-field behaviors of massive MIMO and intelligent reflecting surfaces," *IEEE Open J. Commun. Society*, vol. 1, pp. 1306–1324, Sep. 2020.
- [27] H. Guo, Y.-C. Liang, J. Chen, and E. G. Larsson, "Weighted sum-rate optimization for intelligent reflecting surface enhanced wireless networks," *IEEE Trans. Wireless Commun.*, vol. 19, no. 5, pp. 3064–3076, May. 2020.
- [28] C. Hu and L. Dai, "Two-timescale channel estimation for reconfigurable intelligent surface aided wireless communications," *IEEE Trans. Commun. (early access article)*, Apr. 2021.
- [29] J. An, L. L. Wang, L. Gan, and L. Hanzo, "Optimal pilot power based channel estimation improves the throughput of intelligent reflective surface assisted systems," *IEEE Trans. Veh. Technol.*, vol. 69, no. 12, pp. 16 202–16 206, Dec. 2020.
- [30] S. Ma, W. Shen, J. An, and L. Hanzo, "Wideband channel estimation for IRS-aided systems in the face of beam squint," *IEEE Trans. Wireless Commun. (early access article)*, Apr. 2021.

- [31] S. Gong, Z. Yang, C. Xing, J. An, and L. Hanzo, “Beamforming optimization for intelligent reflecting surface-aided SWIPT IoT networks relying on discrete phase shifts,” *IEEE Internet Things J*, vol. 8, no. 10, pp. 8585–8602, May 2020.
- [32] D. Dardari, “Communicating with large intelligent surfaces: Fundamental limits and models,” *IEEE J. Sel. Areas Commun.*, vol. 38, no. 11, pp. 2526–2537, Nov. 2020.